
11-15-2021

Molecular Design of Polymer Coatings Capable of Photo-Triggered Stress Relaxation via Dynamic Covalent Bond Exchange

Autumn M. Mineo
University of Massachusetts Amherst

Maren E. Buck
Smith College, mbuck@smith.edu

Reika Katsumata
University of Massachusetts Amherst

Follow this and additional works at: https://scholarworks.smith.edu/chm_facpubs

 Part of the [Chemistry Commons](#)

Recommended Citation

Mineo, Autumn M.; Buck, Maren E.; and Katsumata, Reika, "Molecular Design of Polymer Coatings Capable of Photo-Triggered Stress Relaxation via Dynamic Covalent Bond Exchange" (2021). Chemistry: Faculty Publications, Smith College, Northampton, MA.
https://scholarworks.smith.edu/chm_facpubs/22

This Article has been accepted for inclusion in Chemistry: Faculty Publications by an authorized administrator of Smith ScholarWorks. For more information, please contact scholarworks@smith.edu



Pushing the boundaries
of chemistry?
It takes
#HumanChemistry

Make your curiosity and talent as a chemist matter to the world with a specialty chemicals leader. Together, we combine cutting-edge science with engineering expertise to create solutions that answer real-world problems. Find out how our approach to technology creates more opportunities for growth, and see what chemistry can do for you at:

[evonik.com/career](https://www.evonik.com/career)



RESEARCH ARTICLE

Molecular design of polymer coatings capable of photo-triggered stress relaxation via dynamic covalent bond exchange

Autumn M. Mineo¹  | Maren E. Buck²  | Reika Katsumata¹ 

¹Department of Polymer Science and Engineering, University of Massachusetts Amherst, Amherst, Massachusetts, USA

²Department of Chemistry, Smith College, Northampton, Massachusetts, USA

Correspondence

Reika Katsumata, Department of Polymer Science and Engineering, University of Massachusetts Amherst, 120 Governors Dr, Amherst, MA 01003, USA.
Email: rkatsumata@umass.edu

Funding information

GAANN Fellowship; University of Massachusetts-Amherst

Abstract

Polymer coatings are frequently used to modify surface properties of inorganic substrates. However, the disparity in physical properties between polymer film and substrate often leads to residual stress development, which can be deleterious to the overall performance of coated materials. This work reports the molecular design of polymer films that dissipate stress upon irradiation with ultraviolet (UV) light. These polymers are synthesized by post-polymerization modification of the reactive polymer, poly(2-vinyl-4,4-dimethyl azlactone), to introduce dynamic crosslinks capable of light-initiated addition transfer fragmentation chemistry. Using a custom-built optical cantilever, contrasting film stress responses are observed between films containing dynamic bonds and analogous control films after UV light irradiation, which indicate successful stress relaxation. Further experiments demonstrate the complete relaxation of residual stress in dynamic films after an extended exposure, thereby generating a “stress-free” film. Films fabricated using this approach can be easily tailored to incorporate additional moieties to introduce desired surface properties for future application in a wide array of coatings.

KEYWORDS

azlactone, dynamic covalent bond, polymer coating, residual stress, stress relaxation

1 | INTRODUCTION

Surface properties, such as antifouling,^{1,2,3,4,5} corrosion resistance,^{6,7} adhesion,^{8,9} electrochemistry,^{10,11} wettability,^{12,13,14} and light absorption,¹⁵ are commonly modified by the application of polymer coatings to base material. Despite the benefits that polymer coatings offer, residual stresses build at the coating/substrate interface. Typically applied in a liquid phase, polymer films undergo solidification after deposition, which results in the contraction of the film constrained by adhesion to the substrate.^{16,17,18} Such volumetric reduction from film solidification and solvent evaporation introduces shrinkage stresses. Additional

temperature changes during processing introduce thermal stresses rooted in thermal expansion coefficient differences between film and substrate.^{16,19} Together, the summation of shrinkage and thermal stresses constitute residual film stress (generally on the order of MPa), which can lead to material defects, such as curling^{20,21} and crack formation.^{22,23,24} Residual stress is generally reduced below a critical coating strength to avoid these defects by optimizing processing conditions, such as annealing temperature and post-annealing cooling rate.^{25,26,27}

In contrast to these rigorous and system specific methods for minimizing residual stress, dynamic bond

chemistry provides a potentially universal approach for controlling film stress. Although there are many examples of stimuli-responsive dynamic covalent chemistries, such as thermo-reversible Diels-Alder cyclization²⁸ and pH-responsive imine formation,²⁹ photo-triggered radical-mediated addition-fragmentation chain transfer (AFT) is particularly attractive because of its relatively fast reaction kinetics and ability to be temporally and spatially controlled. Of specific advantage for application in polymer coatings, photo-triggered AFT eliminates the potential of further thermal stresses complicating material relaxation, which would be inherent to a thermally-initiated system.

Despite the complimentary attributes of AFT chemistry for application in polymer films, this type of photo-triggered bond exchange has not been explored as a means to control residual stress. Similar to conventional reversible addition fragmentation chain transfer (RAFT) reactions with dithioesters and trithiocarbonates, AFT chemistry with allyl sulfides possesses the stability of a covalent bond while maintaining radical reactivity.³⁰ As a radical process, AFT bond rearrangement occurs rapidly, where each photon absorbed may result in a cascade of bond exchanges, but the total number of cleaved bonds at any one time is kept relatively low.³¹ The radical reactivity of allyl sulfides presents an intrinsic synthetic challenge for its incorporation into polymeric materials, as conventional controlled radical polymerization methods cannot be used. Previous work has tackled this challenge by using unconventional polymerization techniques, such free radical ring opening polymerization,³² and copper-catalyzed azide-alkyne cycloaddition step-growth polymerization,³³ with specially prepared monomers. However, these synthetic tactics are limited by poor control over molecular weight and ease of copolymerization, which would be necessary to incorporate additional film properties.^{34,35} Previous work has also demonstrated the stress-managing potential of AFT chemistry in polymer glasses,³³ gel networks,³⁶ and in polymer composites.³⁷ All of these studies examined stress relaxation of bulk material after light exposure with an applied external strain. However, these studies have not investigated how AFT bond exchanges may relax residual stress in a polymer coating accrued during the curing and annealing processes of film fabrication.

In this work, we aim to systematically study the relationship between photo-triggered AFT bond exchange of allyl sulfides and the relaxation of film stress (Figure 1). Unlike previous synthetic strategies to include allyl sulfide functionality by novel monomer synthesis, we rely on post-polymerization modification to introduce dynamic bonds. Post-polymerization modification is a useful synthetic technique, which allows a variety of functional moieties to be added to a starting polymer structure.^{38,39} Although poly(azlactone)s are not commonly used in commercial coatings, these starting structures have been widely used in

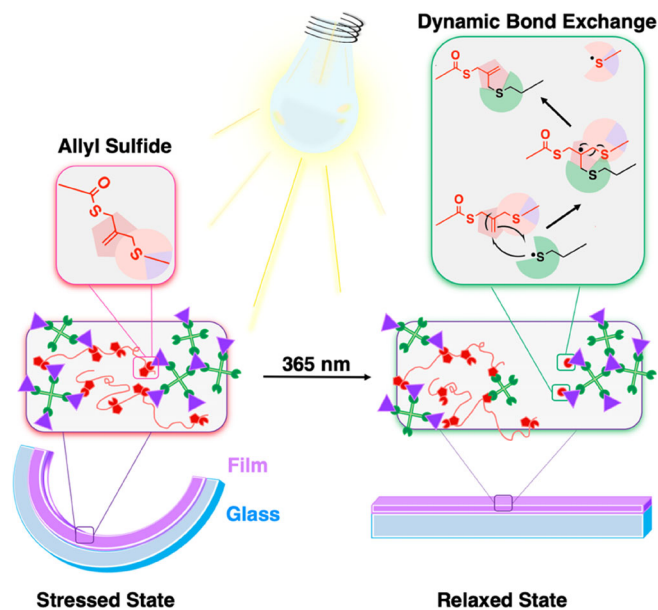


FIGURE 1 Schematic illustration depicting molecular rearrangement by photo-initiated allyl sulfide bond exchange and corresponding macroscopic film-substrate relaxation

academic research because of their practically limitless potential to be chemically tailored by post-polymerization modification.^{40,41,42} Poly(2-vinyl-4,4-dimethyl azlactone) (PVDMA) is an ideal building block as it is synthesized by conventional controlled radical polymerization techniques,⁴³ and undergoes “click-like” ring opening functionalization with a variety of nucleophiles without generating byproducts.^{44,45} By post-polymerization modification, we prepared a library of polymers with five different loadings of allyl dithiol and corresponding control polymers functionalized with a non-dynamic synthetic analogue to investigate the effect of dynamic bond concentration on stress relaxation. We determined film stress from film-substrate curvature monitored by a custom-build optical cantilever with the thin film approximation of the Stoney equation.^{17,19} In contrast to the tensile testing conducted in previous stress relaxation work,^{33,37} an optical cantilever probes interfacial stress while the test material is coated on a substrate, allowing for direct observation of residual stress. The synthetic design explored in this work provides a versatile molecular platform for introducing stress relaxation, where azlactone functionalization may be tailored to impart additional film properties.

2 | RESULTS AND DISCUSSION

2.1 | Synthetic strategy

To investigate the effects of alkyl (covalent bond) and allyl (dynamic covalent bond) sulfide functionality on film stress

relaxation, we modified an azlactone-based polymer to generate a library of polymers with identical molecular weight distributions and various thiol concentrations of both sulfide species. PVDMA is a model starting macromolecular scaffold due to its ability to undergo “click-like” post-polymerization reactions by ring opening nucleophilic attack (Figure 2). All 10 final polymer products (R1-5_P and R1-5_A) were prepared from the same parent PVDMA stock, in order to ensure identical molecular weight distributions (Figure S1). PVDMA was synthesized by atom transfer radical polymerization to achieve modest dispersity ($M_n = 4.2$ kDa, $\bar{D} = 1.32$, Figure S6). Two consecutive post-polymerization reactions were conducted to vary sulfide loading in a controlled manner. Amidation of PVDMA was conducted with five equivalences of phenethylamine (PEA) to yield R1-R5, where R1 has the highest equivalence of PEA (0.83) and R5 has the lowest equivalence of PEA (0.63). Successful amidation of PVDMA with PEA introduced unique aromatic environments, which are easily observed by nuclear magnetic resonance (NMR) to determine residual azlactone concentration. Following amidation, the five intermediate products were each divided into two reaction streams, one with the control group alkyl sulfide, 1,3-propane dithiol (P), and one with the test group allyl sulfide, 2-methylene-1,3-propanedithiol (A), and reacted to full azlactone functionalization. Amidation with PEA was conducted before thioesterification in order to decrease azlactone concentration and sufficiently reduce the likelihood of unwanted nucleophilic crosslinking, as both the control dithiol P and test dithiol A are di-nucleophiles. With this reaction sequence of amidation followed by thioesterification, there was no evidence of crosslinking (i.e. no viscosity changes or solubility changes).

Evidence of successful PVDMA amidation is observed in both ^1H NMR and Fourier transform infrared (FT-IR) spectra of R1-R5 (Figure 3). ^1H NMR reveals the introduction of new aromatic environments (δ 7.20 ppm) from added PEA functionality, which decreases from R1 to R5 effectively corresponding with the PEA equivalence added to the five reactions (inset in Figure 3(A), accompanying Figures S7–S11). FT-IR spectra depict a decrease in azlactone carbonyl intensity (1819 cm^{-1}) inversely matching the PEA loadings observed by ^1H NMR (Figure 3(B)), where R1 has the lowest absorbance at this wavenumber. FT-IR also reveals the emergence of amide peaks (3300 , 1670 , and 1530 cm^{-1}) verifying successful amidation. Additionally, ^{13}C NMR spectra of R1-R5 show the introduction of an amide environment (δ 175 ppm) and three discrete aromatic environments (δ 139, 128, 126 ppm), while also retaining the initial azlactone ester environment (δ 180 ppm) (Figure S12). Thus, both IR and NMR spectra verify intended amidation with the persistence of residual azlactone groups

necessary for continued functionalization via thioesterification.

Given the anticipated partial functional loadings of PVDMA with PEA, all amidation products (R1-R5) were divided into two reaction sequences and fully functionalized with either propane dithiol (P) or allyl dithiol (A) (Figure 2(C)). IR spectra of all final products demonstrate the elimination of residual azlactone as evidenced by the disappearance of the carbonyl peak at 1819 cm^{-1} (Figure 4). Consistent with the elimination of the azlactone carbonyl peak in IR, ^{13}C NMR reveals the same elimination of the azlactone carbonyl environment (δ 180 ppm) (Figures S20 and S27). Evidence of an unintended reaction with ambient water is observed as carboxylic acid absorbance at 1720 cm^{-1} ,⁴⁶ however the presence of hydrolysis is complicated by an overlapping peak at 1730 cm^{-1} from the ester chain end.⁴⁷ The degree to which unwanted hydrolysis has occurred is thought to be minimal, as there are no carboxylic acid environments observed in either ^{13}C or ^1H NMR (Figures S15–S27). Therefore, notwithstanding the presence of minor hydrolysis, quantitative thiol loading may be assumed by the elimination of azlactone functionality.

2.2 | Film fabrication

We employed visible light-initiated radical thiol-alkene coupling to produce crosslinked films ($\sim 125\text{ nm}$ thick) coated on glass coverslips ($\sim 110\text{ }\mu\text{m}$ thick) and UV light-initiated AFT chemistry to enable stress relaxation (Figure 5). Crosslinked networks were prepared with either allyl sulfide functionalized polymers to impart dynamic covalent bonding (Figure 5(B)), or with analogous alkyl sulfide functionalized polymers to act as an appropriate control group lacking dynamic bonds (Figure 5(A)). All films in this work were prepared via spin coating from solutions composed of stoichiometric amounts of thiol to alkene, where $\sim 10\text{ wt\%}$ of the resulting network is composed of thiol functionalized polymers, and the majority of network is composed of assisting crosslinking agents three-arm alkene, 1,3,5-triallyl-1,3,5-triazine-2,4,6-(1H,3H,5H)-trione (TATATO), and four-arm thiol, pentaerythritol tetra(3-mercaptopropionate) (PETMP). Films were first exposed to a curing dose of visible light ($400\text{--}500\text{ nm}$, 435 J/cm^2) larger than those previously reported in literature.³⁷ The curing process and subsequent annealing process determined the initial residual stress in the film due to volumetric shrinkage of the film relative to the substrate, which is depicted as sample curvature in Figure 5. A second irradiation dose of UV light (365 nm) activates additional embedded photo-initiator enabling dynamic bond exchange in the test films. We

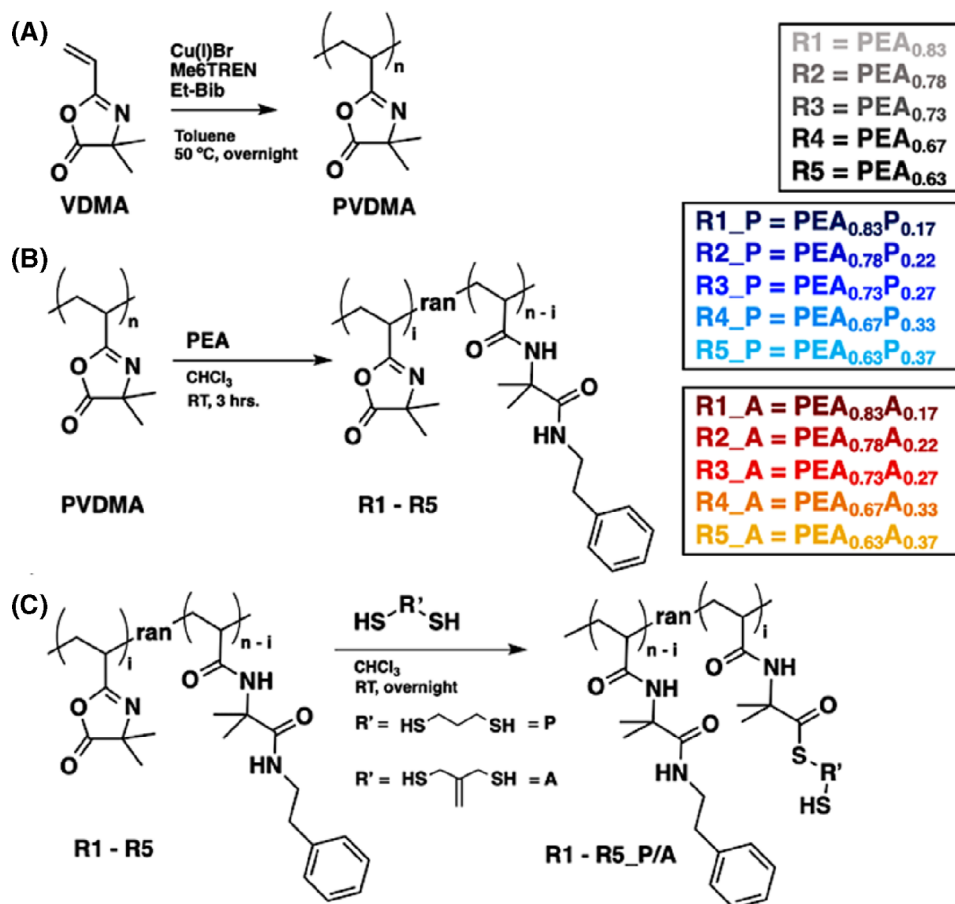


FIGURE 2 (A) Copper mediated polymerization of 2-vinyl-4,4-dimethyl azlactone (VDMA); (B) post-polymerization functionalization of PVDMA via nucleophilic attack with five different equivalences of phenethylamine (PEA) yielding products R1-R5; (C) thioesterification of residual pendant azlactones with either propane dithiol (P) or allyl dithiol (A) yielding products R1-R5_P and R1-R5_A. (The subscripts in the naming color key indicate the molar percentages of each functional loading. See the experimental section for greater detail)

hypothesized that UV-initiated AFT bond exchange within the test films would facilitate the relaxation of residual stress, depicted as the elimination of sample curvature, while control samples lacking dynamic bonds would retain their initial stress. This approach allows for systematic comparison between the control and test films and directly isolates the effect of molecular rearrangement through dynamic bond exchange.

2.3 | Stress relaxation

With the synthesis of five differently alkyl thiol loaded control polymers (R1-5_P) and five corresponding allyl thiol loaded test polymers (R1-5_A), crosslinked films were prepared to investigate stress relaxation behavior (Figure 5). Initial stress at the film-substrate interface is a result of sample curing and cooling from annealing (100°C) to testing (20°C) temperatures, with both processes resulting in volumetric film shrinkage relative to the substrate. Adhesion between the film and substrate prevents film shrinkage along the contact dimensions, which causes upward concavity in the sample with the film occupying the top surface. For simplicity, we assigned upward concavity a positive sign. Samples are

loaded as a cantilever beam into a custom-built laser deflection instrument, which contains a top exposure window for UV dosing and a bottom window for sample position monitoring (Figure 6(A), additional detail see experimental section and Figures S31-S34). Substrate deflection is monitored as a function of time through three exposure cycles at room temperature. Representative deflection data of the films with the highest concentration of sulfide, R5_P and R5_A, are shown in Figure 6(B), and additional data is found in Figures S38-S42. We observe the control film (R5_P) maintaining a nearly constant deflection throughout the 2-h testing period, whereas the test film (R5_A) demonstrated sustained negative deflection that increases with exposure. Negative deflection is consistent with a reduction in a sample's starting curvature, corresponding to a reduction in film stress. From this analysis, we can understand the observed negative deflection in the test sample as the relaxation of initial stress. Data collected during active UV exposure are excluded due to optical interference generating a false deflection signal on the photodetector (Figure S35).

To estimate the initial stress prior to relaxation, we conducted an additional experiment, in which samples were loaded into the laser deflection instrument directly

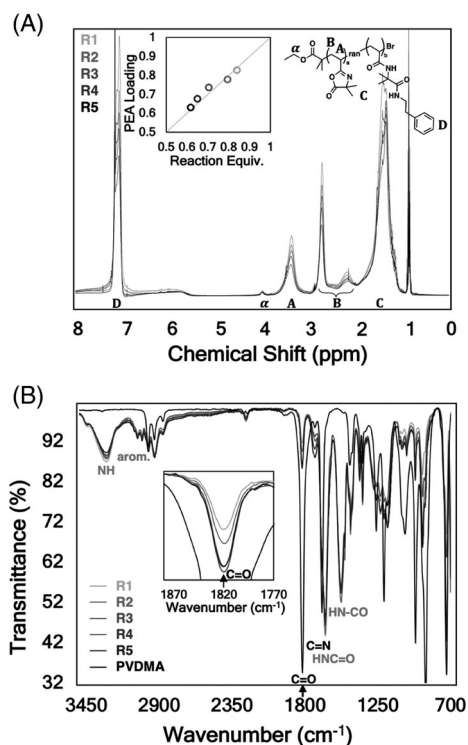


FIGURE 3 (A) ^1H NMR spectra of products R1-R5 demonstrating decreasing aromatic intensity from R1 to R5; inset graph depicts correlation between PEA reaction equivalences relative to azlactone functionality and PEA loading based on aromatic proton integration (environment D relative to α). (B) FT-IR spectra of starting polymer PVDMA (black) and functionalized intermediates R1-R5 (gray); inset showing increasing residual azlactone intensity (1819 cm^{-1} indicated by arrow) from R1 to R5

after spin coating, such that sample curvature was monitored during curing. Observation of sample deflection (ϵ) with visible light exposure allowed us to monitor the magnitude and direction of sample curvature (R) as crosslinking occurred, where l is the cantilever length ($\sim 45\text{ mm}$) and A (~ 6.3) is an empirical constant unique to our testing geometry (Equation (1), additional detail in experimental section and Figure S33). Sample curvature was used to calculate film stress (σ_f) using the thin film approximation of the Stoney Equation,¹⁹ which only requires film thickness ($d_f \sim 125\text{ nm}$) as an input parameter and known physical properties of the glass substrate ($E_s = 72.9\text{ GPa}$,⁴⁸ $d_s = 110\text{ }\mu\text{m}$, $\nu_s = 0.208$)⁴⁹ (Equation 2). The Stoney equation is independent of adhesion strength as long as the coating does not delaminate from the substrate (i.e. perfect contact), which is confirmed by optical microscopy for our samples (Figure S29).

$$\frac{1}{R} = \frac{2}{l^2} \frac{\epsilon}{A} \quad (1)$$

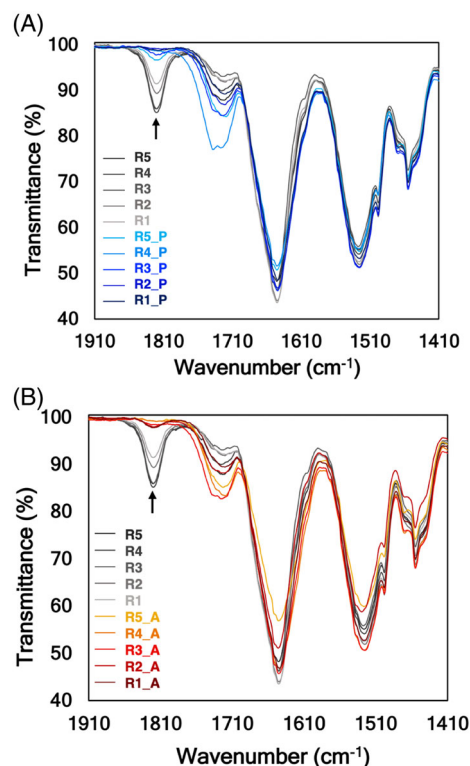


FIGURE 4 FT-IR spectra demonstrating the reduction of residual azlactone intensity (1819 cm^{-1} indicated with an arrow) through the reaction of R1-R5 with propane dithiol (A) and allyl dithiol (B)

$$\sigma_f \approx \frac{1}{6Rd_f} \frac{E_s d_s^2}{(1 - \nu_s)} \quad (2)$$

Using these equations, we examined film stress development in a control and test film through six visible light exposure cycles to complete crosslinking (final dose equivalent to the dosage discussed in Figure 2) and an additional UV exposure for stress relaxation (Figure 7). The curvature of both the control and test film increases positively with additional visible light exposure, which is consistent with our expectation that sample curvature is caused by film shrinkage relative to substrate during cure. As both films approach a cumulative dose of $\sim 435\text{ J/cm}^2$, the film stress reaches a plateau, indicating nearly complete crosslinking. We note the difference in curing stress between control and test samples and hypothesize the observed dissimilarity may be due to differences in mechanical properties between these films or may stem from dynamic bond exchange in the test film during curing. Nevertheless, the maximum stress accumulated in the test film during crosslinking (1.08 MPa) is an important benchmark for the subsequent relaxation studies, although, the other samples discussed in the

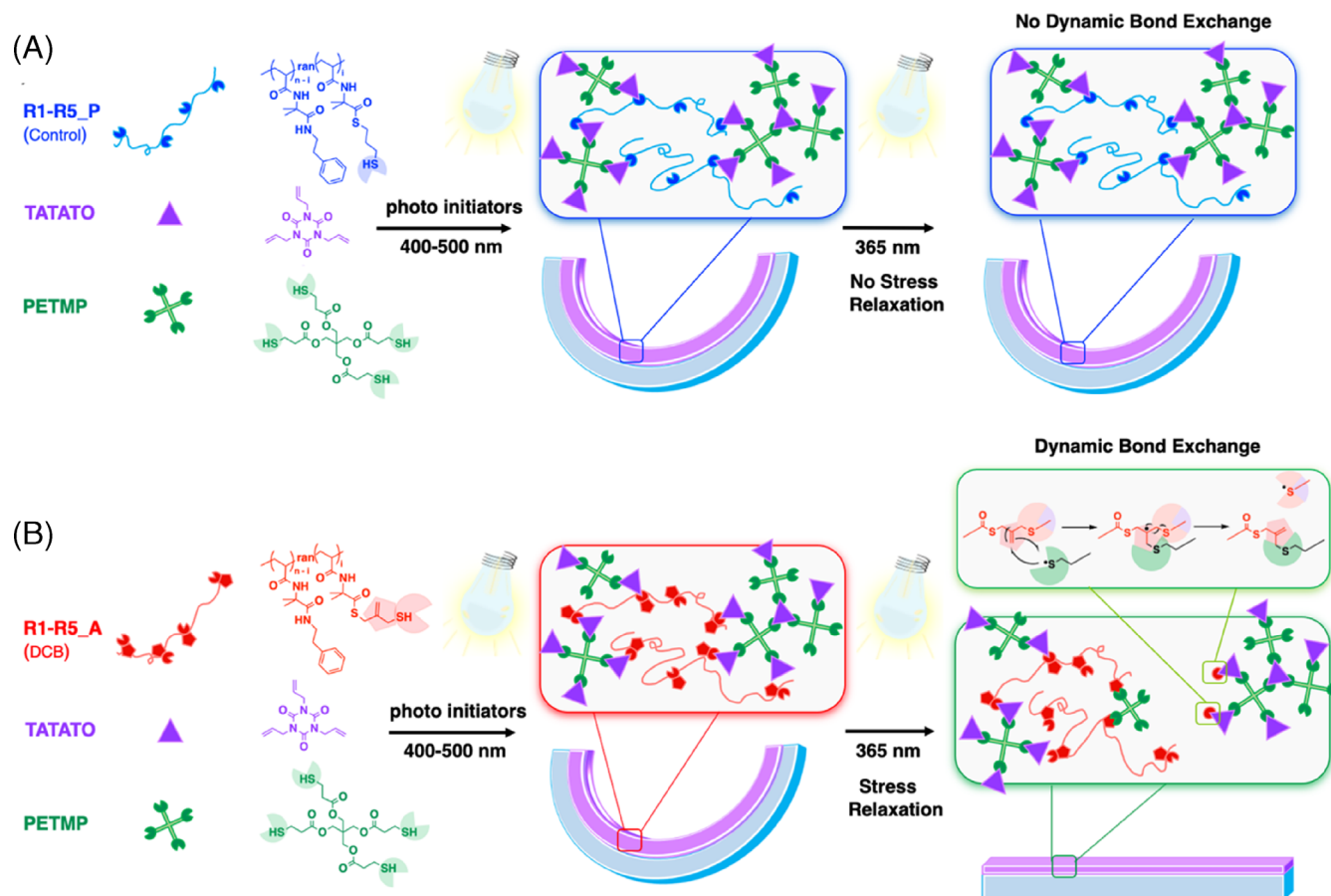


FIGURE 5 Two-step exposure scheme for film synthesis depicting initial visible light initiated thiol-ene network formation (400–500 nm, 10 min, 730 mW/cm²), followed by UV exposure (365 nm, 10 min, 115 mW/cm²) to activate molecular rearrangement. Control network (A) lacks the dynamic covalent bond moiety and cannot exchange network bonds to relax stress, whereas dynamic test network (B) can exchange dynamic bonds through UV initiated AFT type chemistry and relax film stress

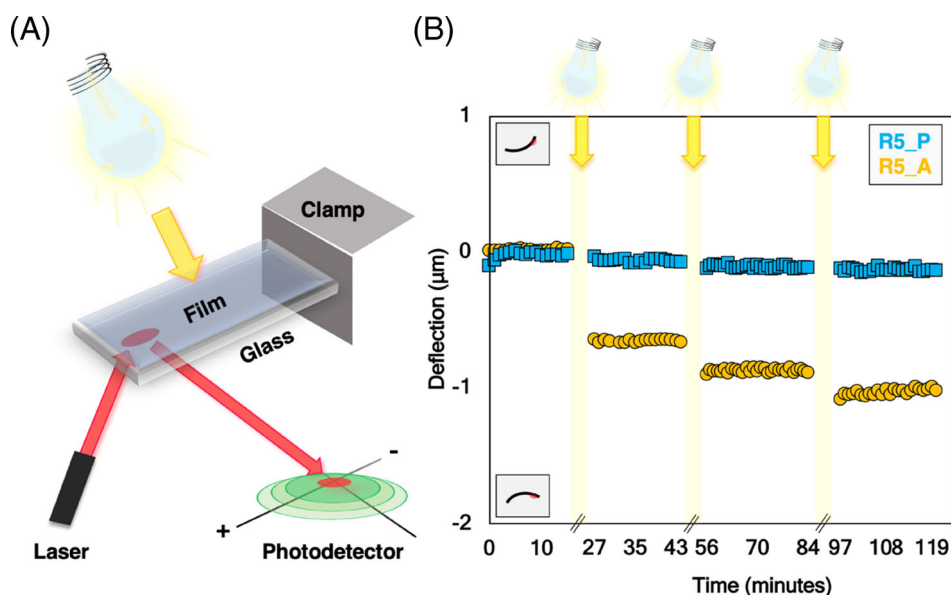


FIGURE 6 (A) Schematic of the custom-made optical cantilever instrument used to monitor sample deflection with time; (B) time versus deflection data of film samples R5_P (blue squares) and R5_A (yellow circles) through three exposure cycles with periods of irradiation (10 min, ~115 mW/cm²) indicated with yellow arrows

work likely have higher residual stresses as they were taken through an additional step of vacuum annealing. During the subsequent UV dose, we observed the film stress of the test film relaxed back to pre-curing

conditions, while the control film retained the stress accrued during sample curing. This experiment demonstrates that dynamic bond exchange effectively relaxes film stress to a “stress-free” state.

By examining film deflection through three UV exposures at room temperature, we observed distinct differences in stress relaxation between test films containing allyl sulfide functionality and control films (Figure 8(A)). Unfortunately, samples from reaction series 1 and 2 were incompletely cured as processing and testing conditions were fully realized only after their fabrication; for completeness, their exposure behavior is included in the supplementary information (Figures S38–39). With products from reaction series 3–5, we observed a difference between control sample (P) and test sample (A) post-exposure behavior. All control samples experience a slight increase in film stress with exposure, which can be explained by additional crosslinking during exposure (Figure 8(A)). In contrast, test samples experience incremental decreases in film stress with exposure. The

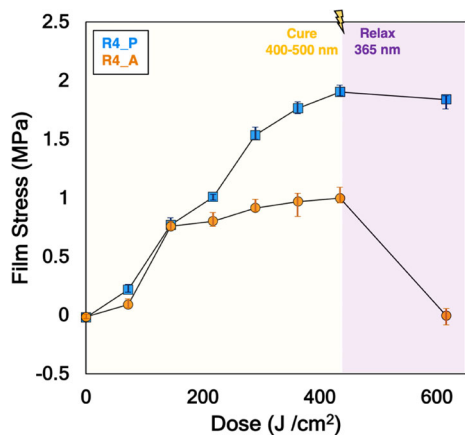
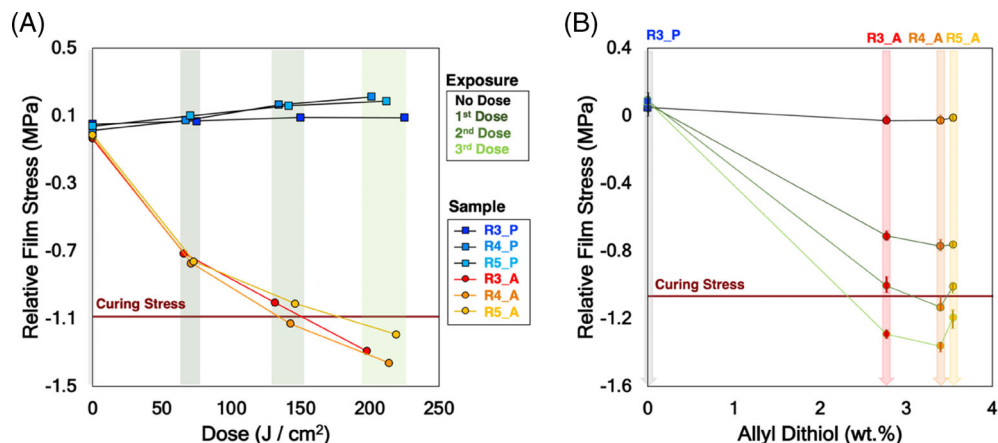


FIGURE 7 Demonstration of curing stress development in control film (R4_P, blue squares) and test film (R4_A, orange circles) during six visible light exposures (400–500 nm, 181 mW/cm², 400 s), and relaxation behavior of R4_P and R4_A after one UV exposure (365 nm, 454 mW/cm², 400 s). Error bars represent the largest and smallest values observed post exposure (the SD is smaller than the size of each data point)

FIGURE 8 Relative film stress in product series R3, R4, and R5 plotted with increasing UV dose (A) and concentration of allyl dithiol (B). Green bars (A) and green connecting lines (B) indicate the exposure number. Vertical arrows (B) represent the same sample with increasing exposure. Error bars (B) represent the largest and smallest values observed post exposure (the SD is smaller than the size of each data point)



observed amount of stress relaxation in test samples matches in magnitude with the curing stress demonstrated in Figure 7 (1.08 MPa); however, all test films relax further than this value, which indicates a larger initial residual stress in these samples from the additional annealing process. Stress relaxation in all test samples follows an exponential decay curve with continued exposure, which matches intuitively with both the complete relaxation of initial stress and the depletion of embedded photoinitiator. Future experiments will attempt to decouple these variables by thermally inducing additional film stress after relaxation events. We observed the complete relaxation in sample R1_A after a UV dose of ~350 J/cm² (Figure S44). The dose required for full stress relaxation depends on both the thermal history and curing stress. Nevertheless, ~350 J/cm² is a reasonable estimate of the highest dosage needed to obtain “stress-free” samples.

One of our hypotheses in this work was that by varying the allyl dithiol loading in the polymer component of the films, the rate of stress relaxation would be different. However, we did not observe a clear trend between allyl sulfide concentration (allyl dithiol wt%) and post-exposure film stress (Figure 8(B)). Although, this may be due to the relatively low concentration of polymer in the resulting films (~10 wt% in the dry film), as well as the narrow variation in the allyl dithiol loading, future experiments will study film stress relaxation with more diverse allyl sulfide concentrations to elucidate potential differences in material relaxation on shorter time scales and at under larger initial stresses.

3 | CONCLUSION

In this work, we synthesized a series of alkyl and allyl sulfide containing polymers and demonstrated that the inclusion of allyl sulfide groups introduces stress relaxation by photo-triggered dynamic bond exchange. PVDMA acted as

an ideal starting framework for two consecutive nucleophilic functionalization reactions, which allowed us to precisely control sulfide loading. Through this work, we highlight the advantages of using post-polymerization modification as a synthetic strategy to generate a variety of sulfide containing polymers with identical backbone architectures. The potential of photo-triggered residual stress relaxation is demonstrated by the complete relaxation of curing stress after one UV exposure, generating a “stress-free” film. These results validate our synthetic approach for incorporating stress relaxation into a molecular framework and our continued effort to understand the interplay between molecular rearrangement kinetics and macroscopic material relaxation.

4 | EXPERIMENTAL

4.1 | Materials

All chemicals were either synthesized as indicated or purchased from either Fisher or Sigma Aldrich, and used as received unless otherwise stated.

4.2 | Instrumentation

ATR FT-IR spectroscopy was conducted on a Spectrum One FT-IR Spectrometer purchased from Perkin Elmer. All IR spectra are from products cast on the IR crystal as a dilute solution in CDCl_3 unless otherwise specified.

4.3 | Synthesis of 2-vinyl-4,4-dimethyl azlactone (VDMA)

VDMA was synthesized following previously reported methods⁴⁴; ^1H NMR (400 MHz, CDCl_3 , δ): 6.27 (m, 2H, vinylic gem. H), 5.29 (d, 1H, vinyl H), 1.45 (s, 6H, CH_3) (Figure S2).

4.4 | Synthesis of poly(2-vinyl-4,4-dimethyl azlactone) (PVDMA)

PVDMA was synthesized using procedures reported by Fontaine et al. with minor modifications.⁵⁰ VDMA was brought to room temperature and allowed to stir with radical inhibitor removal resin for approximately 5 min. VDMA was passed through a short plug silica column and gravimetrically measured. A clean dry Schlenk flask was charged with VDMA (6.3681 g, 45.8 mmol, 100 equiv.), tris [2-dimethylamino]ethylamine (Me_6TREN) (115.4 mg, 0.5 mmol, 1.1 equiv.), and anhydrous toluene (6.2 ml). The

monomer-ligand solution was taken through five freeze pump thaw cycles and placed under nitrogen. Another clean dry Schlenk flask was equipped with a magnetic stir bar and charged with ethyl 2-bromo-isobutyrate (102.8 mg, 0.5 mmol, 1.1 equiv.) and purified copper bromide (66.7 mg, 0.5 mmol, 0.47 mmol, 1.02 equiv.). The copper flask was then taken through three evacuation/ N_2 charge cycles at -196°C and then placed under heavy N_2 flow. The deoxygenated monomer-ligand solution was transferred to the copper flask under N_2 and together the reaction mixture was taken through six freeze-pump-thaw cycles and then placed under N_2 flow. The reaction solution was allowed to stir at 25°C for 30 min and then taken to reaction temperature of 50°C over the course of 20 min. After 24 h, the reaction mixture was precipitated into hexanes, collected and redissolved in dichloromethane, and passed through a short silica column (3 ml). Polymer was precipitated again in hexanes, collected, and dried under vacuum. ^1H NMR (400 MHz, CDCl_3 , δ): 4.08 (s, 2H, ether H), 2.73 (s, 49H, methylene), 2.09–1.91 (m, 98H, methylene), 1.39 (s, 294H, CH_3); ^{13}C NMR (400 MHz, CDCl_3 , δ): 180.22 (C=O), 163.07 (C=N), 65.47 (C–N), 35.27 (methylene), 24.16 (CH_3) (Figures S3–S4).

4.5 | Matrix assisted laser desorption ionization-time of flight mass spectroscopy (MALDI-TOF MS) of PVDMA

PVDMA was functionalized with methanol prior to MALDI experiments due to its sensitivity to the acidic conditions present in the matrix. PVDMA product was suspended in methanol and allowed to sit at room temperature for 4 days to reach full functionalization. Full functionalization was verified with ATR-FT IR spectroscopy by the elimination of azlactone peak at 1819 cm^{-1} (Figure S5). PVDMA-OMe product was dissolved in chloroform (10 mg/ml) and mixed in varying amounts (polymer to matrix; 1:1–1:10) of matrix solution (300 mg of 2,5-dihydrobenzoic acid: 3 mg of sodium trifluoroacetate/3 ml of acetone). Mass characteristics of PVDMA product were $M_n = 4.2\text{ kDa}$, $M_w = 5.6\text{ kDa}$, $n \sim 33$, $MW_n = 171\text{ g/mol}$, and $\text{Đ} = 1.32$ (Figure S6).

4.6 | Synthesis of R1-R5

All five intermediate products were synthesized from the same starting PVDMA batch, which was divided into five reaction streams and taken through the same synthetic procedure (Figure S1). A clean flask was equipped with a magnetic stirring bar and charged with PVDMA (~250 mg). PVDMA was uniformly dissolved in chloroform (2 ml) and phenethylamine (178–142 mg) was added dropwise with continued stirring. Reactions were allowed to stir closed to atmosphere at room temperature for 3 h.

Reaction mixtures were precipitated in hexanes, collected, and dried overnight under vacuum. While unwanted hydrolysis of azlactone functionality with atmospheric water is a concern when working with PVDMA, storage in a vacuum desiccator proved to be an appropriate strategy to prevent hydrolysis, as a sample of R4 retained initial azlactone functionality at these conditions for over a month (Figure S14). ^1H NMR (400 MHz, CDCl_3 , δ): 7.81 (s, amide H), 7.18 (m, Ar H), 6.01 (s, amide H), 4.07 (s, ester H), 3.44 (s, methylene), 2.77–2.23 (m, methylene), 1.42 (s, CH_3) (Figures S7–S11). ^{13}C NMR (400 MHz, CDCl_3 , δ): 180.7 (azlactone $\text{C}=\text{O}$), 174.66 (amide $\text{C}=\text{O}$), 163.07 (azlactone $\text{C}=\text{N}$), 138.91 (Ar), 128.52 (Ar), 126.10 (Ar), 65.23 (azlactone $\text{C}-\text{N}$), 56.29 (amide $\text{Me}_2\text{-C}-\text{N}$), 40.83 (ethylene), 35.27 (methylene), 24.16 (CH_3) (Figure S12).

4.7 | Synthesis of 3-mercapto-2-(mercaptomethyl)-1-propene (allyl dithiol)

Allyl dithiol was synthesized following previously reported methods with minor changes.³² Bulb to bulb distillation of final product was carried out by assembling clean, dry distillation glassware. Each joint was greased with vacuum grease, and supported with a keck clip. A reflux condenser was flushed with cold water until the system was cool and the collecting flask was held in a liquid nitrogen bath prior to exposure to vacuum with a bleed line open. The bleed line was slowly closed at room temperature. Slowly the temperature of the crude final product was increased from room temperature to $\sim 37^\circ\text{C}$ in two degree increments over the course of 3 h. After 3 h, the crude product flask contained a white solid suspended in a small amount of yellow oil, while the collecting flask contained the intended product, a colorless oil. ^1H NMR (400 MHz, CDCl_3 , δ): 5.03 (s, 2H, vinyl), 3.37 (d, 4H, methylene), 1.51 (t, 2H, SH) (Figure S21).

4.8 | Synthesis of R1-R5_P/A

All final products were directly synthesized from intermediate species (R1–R5) by dividing each intermediate into two reaction streams in which thioesterification was carried out by either 1,3-propane dithiol or synthesized allyl dithiol. A clean flask was equipped with a magnetic stir bar and charged with amidation intermediate (R1–R5) (~ 125 mg) and chloroform (4 ml). Once uniformly dissolved, the reaction was stirred as dithiol (5 mol% excess) was added dropwise. Reactions were closed from atmosphere and allowed to stir at room temperature for 3 days. Final products were precipitated into hexanes, collected, and dried under vacuum overnight. See SI for

^1H NMR (Figures S15–S19, S22–S26), and ^{13}C NMR (Figures S20 and S27).

4.9 | Film fabrication instrumentation

Fisherbrand microscope cover glass (24 mm by 50 mm, thickness of 110 μm) was purchased from Fisher Scientific. Glass cleaning was performed with an ultrasonic bath sonicator (Branson Ultrasonics, CPX3800) and UVO (Jelight, model 18). Films were prepared through spin coating on a spin coater purchased from Ossila. Omnicure model S2000 light source with external filter (400–500 nm), purchased from Lumen Dynamics, was used for sample curing. Ellipsometry was conducted on a Gaertner LSE ellipsometer equipped with a Melles Griot laser source (633 nm). Optical microscopy was conducted on a Zeiss Axioscope model 5 using ZEN 2 core v2.5 software.

4.10 | Film preparation

All casting solutions were prepared such that the molar concentration of thiol to alkene was 1 to 1. Polymer products (R1–R5_P/A) (25 mg, ~ 2 wt%) were uniformly dissolved in anhydrous dimethyl formamide (1.059 ml). Crosslinking agents triallyl-s-triazine-2,4,6(1H,3H,5H)-trione (TATATO) and pentaerythritol tetra(3-mercaptopropionate) (PETMP) (together ~ 14 wt%) were added and uniformly dissolved. Finally two photo initiator species, phenyl bis(2,4,6-trimethylbenzoyl)phosphine oxide (~ 0.8 wt%) and 2,2-dimethoxy-2-phenylacetophenone (~ 0.4 wt%), were uniformly suspended in the casting solution. Each solution was cast onto a cleaned glass slide (24 mm by 50 mm by 110 μm) by spin coating. Glass substrates were cleaned by sonication in reagent grade ethanol for 2 min, dried under nitrogen, and exposed to UVO for 1 min. Coated substrates were then exposed to visible light (400–500 nm, 731 mW/cm^2 , 10 min), and vacuum annealed overnight (~ 5 mbar, 100°C , 24 h). Ellipsometry was performed on the resulting films to determine thickness (Figure S28). Optical microscopy was performed on the resulting films to understand general coating uniformity (Figure S29). Samples were stored at 20°C protected from light until UV exposure testing.

4.11 | Laser deflection analysis instrument

Omnicure model S2000 light source with external filters 320–390 nm, purchased from Lumen Dynamics, was used in sample relaxation studies (~ 115 mW/cm^2 ,

10 min). The laser deflection analysis instrument was built in house using materials acquired from Thorlabs (Kinesis K-Cube Position Sensing Detector Controller KPA101 and lateral effect position sensor PDP90A). Accompanying Thorlabs software was used to understand four quadrant photodetector signal output. Heating and PID temperature monitoring elements were acquired from Omega, and accompanying Platinum software was used to monitor temperature throughout exposure experiments.

Pictures of the LDA setup are provided in the supplementary information (Figures S30-S32). Induced cantilever deflection from the addition of small weights (identical pieces of paper) on a glass cantilever was used to calibrate the LDA instrument, such that the deflection could be measured independently with a micrometer and through the displacement of laser reflection on the photodetector of the LDA instrument. The relationship between these two measurements defines A the empirical constant specific to the LDA geometry (Figure S33). Reliability of our LDA set up was further confirmed by agreement between experimentally measured thermally induced deflection of poly(methyl methacrylate) (PMMA) films with theoretical values predicted from thermal expansion coefficient mismatch between PMMA films and the glass substrate (Figure S34).¹⁹

ACKNOWLEDGMENTS

RK acknowledge financial support from the University of Massachusetts Amherst for starting faculty support. AMM acknowledge financial support through the Graduate Assistance in Areas of National Need (GAANN) Fellowship from the U.S. Department of Education. We acknowledge the previous work done by Thomas Kumlin in the fabrication of our optical cantilever instrument. We thank Professor Thomas McCarthy for providing use of their ellipsometer. We also thank Professor Todd Emrick for providing use of their FT-IR spectrometer. We appreciate the helpful discussions with Professor Alfred J. Crosby.

CONFLICT OF INTEREST

The authors declare no conflicts of interest.

ORCID

Autumn M. Mineo  <https://orcid.org/0000-0002-4489-9711>

Maren E. Buck  <https://orcid.org/0000-0002-1404-8588>

Reika Katsumata  <https://orcid.org/0000-0003-3119-9385>

REFERENCES

- [1] C. Zhao, L. Li, Q. Wang, Q. Yu, J. Zheng, *Langmuir* **2011**, *27*, 4906.
- [2] Y. Chen, D. Liu, Q. Deng, X. He, X. Wang, *J. Polym. Sci. Part Polym. Chem.* **2006**, *44*, 3434.
- [3] T. He, D. Jańczewski, S. Jana, A. Parthiban, S. Guo, X. Zhu, S. S.-C. Lee, F. J. Parra-Velandia, S. L.-M. Teo, G. J. Vancso, *J. Polym. Sci. Polym. Chem.* **2016**, *54*, 275.
- [4] M. E. Barry, E. C. Davidson, C. Zhang, A. L. Patterson, B. Yu, A. K. Leonardi, N. Duzen, K. Malaviya, J. L. Clarke, J. A. Finlay, A. S. Clare, Z. Chen, C. K. Ober, R. A. Segalman, *Macromolecules* **2019**, *52*, 1287.
- [5] A. L. Patterson, B. Wenning, G. Rizis, D. R. Calabrese, J. A. Finlay, S. C. Franco, R. N. Zuckermann, A. S. Clare, E. J. Kramer, C. K. Ober, R. A. Segalman, *Macromolecules* **2017**, *50*, 2656.
- [6] C. K. Tan, D. J. Blackwood, *Corros. Sci.* **2003**, *45*, 545.
- [7] J. W. Truesdell, M. R. Van De Mark, *J. Polym. Sci. Polym. Chem. Ed.* **1982**, *20*, 1899.
- [8] L. Gong, L. Xiang, J. Zhang, J. Chen, H. Zeng, *Langmuir* **2019**, *35*, 15914.
- [9] H. Watanabe, A. Fujimoto, A. Takahara, *J. Polym. Sci. Polym. Chem.* **2013**, *51*, 3688.
- [10] J. Janata, M. Josowicz, *Nat. Mater.* **2003**, *2*, 19.
- [11] J. N. Pagaduan, N. Hight-Huf, A. Datar, Y. Nagar, M. Barnes, D. Naveh, A. Ramasubramaniam, R. Katsumata, T. Emrick, *ACS Nano* **2021**, *15*, 2762.
- [12] B. Xin, J. Hao, *Chem. Soc. Rev.* **2010**, *39*, 769.
- [13] B. Jiang, H. Pang, *J. Polym. Sci. Polym. Chem.* **2016**, *54*, 992.
- [14] M. Kanidi, A. Papagiannopoulos, A. Skandalis, M. Kandyla, S. Pispas, *J. Polym. Sci. Part B Polym. Phys.* **2019**, *57*, 670.
- [15] Y. Liang, D. Feng, Y. Wu, S.-T. Tsai, G. Li, C. Ray, L. Yu, *J. Am. Chem. Soc.* **2009**, *131*, 7792.
- [16] L. F. Francis, A. V. McCormick, D. M. Vaessen, J. A. Payne, *J. Mater. Sci.* **2002**, *37*, 4717.
- [17] C. Petersen, C. Heldmann, D. Johannsmann, *Langmuir* **1999**, *15*, 7745.
- [18] R. Katsumata, S. Ata, K. Kuboyama, T. Ougizawa, *J. Appl. Polym. Sci.* **2013**, *128*, 60.
- [19] M. Ohring, *Materials Science of Thin Films: Deposition and Structure*, 2nd ed., Academic Press, San Diego, CA **2002**.
- [20] K. N. Christodoulou, E. J. Lightfoot, R. W. Powell, *AIChE J.* **1998**, *44*, 1484.
- [21] B. A. Morris, *J. Plast. Film Sheet.* **2003**, *19*, 31.
- [22] T. Y. Tsui, A. J. McKerrow, J. J. Vlassak, *J. Mater. Res.* **2005**, *20*, 2266.
- [23] W.-P. Vellinga, A. Fedorov, J. T. De Hosson, *Thin Solid Films* **2008**, *517*, 841.
- [24] G. Reiter, M. Hamieh, P. Damman, S. Sclavons, S. Gabriele, T. Vilmin, E. Raphaël, *Nat. Mater.* **2005**, *4*, 754.
- [25] K. R. Thomas, U. Steiner, *Soft Matter* **2011**, *7*, 7839.
- [26] K. Ramani, W. Zhao, *Int. J. Adhes. Adhes.* **1997**, *17*, 353.
- [27] M. D. Thouless, *Annu. Rev. Mater. Sci.* **1995**, *25*, 69.
- [28] M. Vauthier, L. Jierry, J. C. Oliveira, L. Hassouna, V. Roucoules, F. Bally-Le Gall, *Adv. Funct. Mater.* **2019**, *29*, 765.
- [29] C. Wang, G. Wang, Z. Wang, X. Zhang, *Chem. A Eur. J.* **2011**, *17*, 3322.
- [30] C. R. Fenoli, C. N. Bowman, *Polym. Chem.* **2014**, *5*, 62.

- [31] C. J. Kloxin, T. F. Scott, B. J. Adzima, C. N. Bowman, *Macromolecules* **2010**, *43*, 2643.
- [32] R. A. Evans, E. Rizzardo, *Macromolecules* **2000**, *33*, 6722.
- [33] N. Sowan, H. B. Song, L. M. Cox, J. R. Patton, B. D. Fairbanks, Y. Ding, C. N. Bowman, *Adv. Mater.* **2021**, *33*, 7221.
- [34] W. Bailey, *J. Polym. J.* **1985**, *17*, 85.
- [35] P. L. Golas, K. Matyjaszewski, *Chem. Soc. Rev.* **2010**, *39*, 1338.
- [36] T. F. Scott, A. D. Schneider, W. D. Cook, C. N. Bowman, *Science* **2005**, *308*, 1615.
- [37] N. Sowan, L. M. Cox, P. K. Shah, H. B. Song, J. W. Stansbury, C. N. Bowman, *Adv. Mater. Interfaces* **2018**, *5*, 1800511.
- [38] M. A. Gauthier, M. I. Gibson, H.-A. Klok, *Angew. Chem. Int. Ed.* **2009**, *48*, 48.
- [39] T. Kubo, C. P. Easterling, R. A. Olson, B. S. Sumerlin, *Polym. Chem.* **2018**, *9*, 4605.
- [40] M. E. Buck, J. Zhang, D. M. Lynn, *Adv. Mater.* **2007**, *19*, 3951.
- [41] J. E. Barringer, J. M. Messman, A. L. Banaszek, H. M. Meyer, S. M. Kilbey, *Langmuir* **2009**, *25*, 262.
- [42] B. S. Lokitz, J. M. Messman, J. P. Hinestrosa, J. Alonzo, R. Verduzco, R. H. Brown, M. Osa, J. F. Ankner, S. M. Kilbey, *Macromolecules* **2009**, *42*, 9018.
- [43] M. E. Buck, D. M. Lynn, *Polym. Chem.* **2012**, *3*, 66.
- [44] M. M. Wancura, Q. Anex-Ries, A. L. Carroll, A. Paola Garcia, P. Hindocha, M. E. Buck, *J. Polym. Sci. Part Polym. Chem.* **2017**, *55*, 3185.
- [45] E. R. Fitzgerald, A. M. Mineo, M. L. Pryor, M. E. Buck, *Soft Matter* **2020**, *16*, 6044.
- [46] T. J. Zimudzi, K. E. Feldman, J. F. Sturnfield, A. Roy, M. A. Hickner, C. M. Stafford, *Macromolecules* **2018**, *51*, 6623.
- [47] L. I. Fockaert, S. Pletincx, D. Ganzinga-Jurg, B. Boelen, T. Hauffman, H. Terryn, J. M. C. Mol, *Appl. Surf. Sci.* **2020**, *508*, 144771.
- [48] R. W. Hoffman, T. E. Mitchell, R. W. Hoffman, *Thin Solid Films* **1987**, *154*, 149.
- [49] N. I. Christensen, *J. Geophys. Res. Solid Earth* **1996**, *101*, 3139.
- [50] D. Fournier, S. Pascual, L. Fontaine, *Macromolecules* **2004**, *37*, 330.

SUPPORTING INFORMATION

Additional supporting information may be found online in the Supporting Information section at the end of this article.

How to cite this article: A. M. Mineo, M. E. Buck, R. Katsumata, *J. Polym. Sci.* **2021**, *59*(22), 2719. <https://doi.org/10.1002/pol.20210464>